Florian Pfaff*, Georg Maier, Mikhail Aristov, Benjamin Noack, Robin Gruna, Uwe D. Hanebeck, Thomas Längle, Jürgen Beyerer, Christoph Pieper, Harald Kruggel-Emden, Siegmar Wirtz, and Viktor Scherer

Real-Time Motion Prediction Using the Chromatic Offset of Line Scan Cameras

Abstract: State-of-the-art optical belt sorters commonly employ line scan cameras and use simple assumptions to predict each particle's movement, which is required for the separation process. Previously, we have equipped an experimental optical belt sorter with an area scan camera and were able to show that tracking the particles of the bulk material results in an improvement of the predictions and thus also the sorting process. In this paper, we use the slight gap between the sensor lines of an RGB line scan camera to derive information about the particles' movements in real-time. This approach allows improving the predictions in optical belt sorters without necessitating any hardware modifications.

Keywords: Sensor-based sorting, line scan camera, bulk material, predictive tracking, chromatic offset

1 Introduction

Automatic sensor-based sorters [1] are a key technology for ensuring quality of food [2, 3], minerals [4], and glass as well as a means for highly efficient waste management [5]. Notably, optical belt sorters are a technology that can be used to sort a wide variety of bulk materials using a dry sorting process, necessitating only few changes to the sorter for differing bulk materials. Due to their universal

***Corresponding Author: Florian Pfaff:** Intelligent Sensor-Actuator-Systems Laboratory (ISAS), Karlsruhe Institute of Technology (KIT), Germany.
Mikhail Aristov, Benjamin Noack, Uwe D. Hanebeck: Intelligent Sensor-Actuator-Systems Laboratory (ISAS), Karlsruhe Institute of Technology (KIT), Germany.
Georg Maier, Robin Gruna, Thomas Längle, Jürgen Beyerer: Fraunhofer Institute of Optronics, System Technologies and Image Exploitation (IOSB), Germany.
Christoph Pieper, Siegmar Wirtz, Viktor Scherer: Department of Energy Plant Technology (LEAT), Ruhr-Universität Bochum (RUB), Germany.
Harald Kruggel-Emden: Mechanical Process Engineering and Solids Processing (MVTA), Technical University Berlin, Germany.

applicability, improving optical belt sorters has an impact on a variety of bulk material sorting tasks.

Current optical belt sorters used in industrial applications, as illustrated in Fig. 1, usually employ line scan cameras, which are imaging sensors that only provide a single line of pixels. By using cameras with high frame rates, one side of the surface of each particle passing by the line scan camera can be fully inspected. The observation of the particle is used both for localizing and classifying the particle of the bulk material.

A common way to perform the separation in optical belt sorters is to target one class of particles using bursts of compressed air to alter the flight paths of these particles. The particles that are hit then land in a different container than the particles that fly unobstructed. The bursts of compressed air are emitted by nozzles aligned orthogonally to the transport direction of the belt.

For the prediction as to when and where a particle will pass the array of nozzles, current systems used in industrial settings assume that all particles move precisely in the transport direction with an identical speed. While many bulk materials exist for which this assumption is sufficiently accurate, so-called uncooperative bulk materials feature a much more differentiated motion behavior and, in general, do not follow a straight motion path even when significant effort is put into enforcing this behavior. In common strategies to alleviate this problem, motion orthogonal to the transport direction is reduced by altering the sorter. But such changes, e.g., using longer belts or using belts with a fluted surface, induce additional costs or have other undesirable implications.

As an alternative to these expensive hardware extensions to alter the motion behavior, we have presented an extension that only requires the use of an area scan camera and appropriate algorithms [6, 7]. In these works, we replaced the line scan camera in the system with an area scan camera to observe the particles travel along the belt. Using multiple observations of a particle, we can predict the time and place the particle will pass the separation mechanism with higher precision—an approach that we refer to as predictive tracking. We have validated this approach using real image data and also using simulations in our subsequent works [8, 9] and presented ways to maintain real-time capabilities in [10].

The predictive tracking approach has a variety of benefits that go beyond improving the accuracy of the separation. The classification can be enhanced via the use of multiple observations, e.g., by utilizing the increased amount of visual data and the characteristics of the motion behavior.

In this paper, we present a novel approach for which no area scan camera is required. In our new approach called ColorTrack, we use the offset between different color channels of an RGB line scan camera to derive information about the particle's motion behavior. This approach features some of the advantages

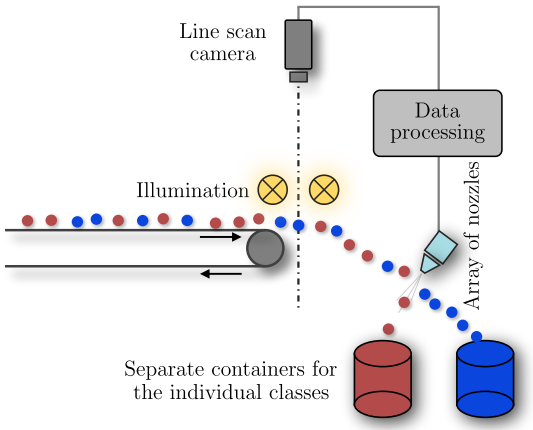

Fig. 1. Illustration of an optical belt sorter.

of the predictive tracking and can be used in real-time on existing optical belt sorters equipped with a line scan camera with a compatible sensor layout.

2 Key Idea

To record color images, incoming light is usually filtered in such a way that individual pixel sensors of an image sensor only capture certain wavelengths. The information of multiple pixels is then combined into one pixel featuring a mixture of the colors red, green, and blue. For area scan cameras, a popular scheme to filter the light and combine multiple monochromic pixels into one RGB pixel is the so-called Bayer filter [11]. As an individual pixel sensor capturing one color channel is square, four pixel sensors can be combined to cover a square region on the chip. Out of these four sensors, one captures the color red, one the color blue, and two capture the color green[1].

For line scan cameras, similar challenges arise as the RGB pixels are also generated using multiple pixels capturing only certain wavelengths. However, as line scan cameras only record a one-dimensional array of RGB pixels, different requirements apply and patterns designed specifically for line scan cameras are commonly used. Three frequently used patterns for RGB line scan cameras

1 The color green is commonly deemed more important than red and blue because the human eye is more sensitive to green [11].

that can be used in our new approach are the so-called bilinear, trilinear, and quadlinear patterns [12, 13].

In the trilinear pattern [14, 15] illustrated in Fig. 2a, three separate lines for each color are arranged in parallel. Some cameras are also available with a quadlinear pattern shown in Fig. 2b, which includes a fourth line for near infrared or monochrome pixels [16, 17]. In the bilinear pattern [18, 19] illustrated in Fig. 2c, a single line of pixels alternatingly capturing blue and red is placed beside a line of pixels that only captures green. Line scan cameras using a bilinear pattern commonly feature a lower resolution than those using a trilinear or quadlinear pattern as pixels of two colors alternate along a single line.

A very important feature of the sensor patterns are the gaps between the individual lines of pixels. In order to obtain an RGB pixel using three pixel sensors capturing different wavelengths, the visual information is usually combined with a certain temporal offset that depends on the speed of the bulk material moving in the transport direction. A weakness is that if the assumption about the speed is not sufficiently precise or if there is movement orthogonal to the transport direction, the color information cannot be combined seamlessly.

There are, however, color line scan cameras for which this usually undesirable property does not exist. For one, there are cameras using a monoline pattern [20], which is a simple round robin pattern as shown in Fig. 2d. Another solution is to use a prism to distribute the incoming light to three separate arrays of pixel sensors. But this solution, while also applicable to area scan cameras, is costly and thus used only infrequently.

In this paper, we focus on line scan cameras using a bi-, tri-, or quadlinear pattern and use their usual weakness to our advantage. First, we disable any temporal offset in the combination of the color channels. Second, we assume that all particles are visible in all color channels, allowing for multiple observations of each particle. Due to the spatial offset of the multiple lines, we observe the particle at two or three different points in time.

In our ColorTrack approach, we use these multiple observations of each individual particle to approximate its velocity. The first step is to find the particle of the bulk material in at least two color channels and to correctly associate the observations to the respective particle. By approximating all possible flight paths with a curved plane as shown in Fig. 3, we can project the particle's centroid in each channel into world coordinates. The centroid is used to take into account that non-rotationally symmetric particles may be viewed in slightly different orientations and that the translatory part of a motion can be described by the motion of its centroid.

Using the different color channels, we obtain the coordinates of the particle's centroid at multiple points in time. Since we have a known sampling rate, we

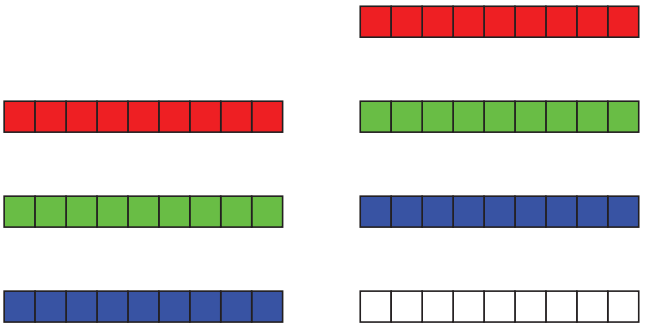

(a) Illustration of the trilinear layout. The green line is usually placed in the middle.

(b) Illustration of the quadlinear layout. The fourth line serves to record monochrome images or to capture near-infrared wavelengths.

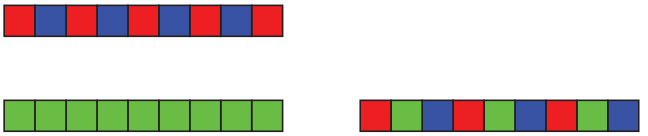

(c) Illustration of the bilinear (also called dual line) layout. Commonly, the pixels for red and blue alternate along the mixed sensor line.

(d) Illustration of the monoline layout.

Fig. 2. Visualizations of the different sensor layouts. The gaps between the lines are kept small for illustration purposes and are usually wider.

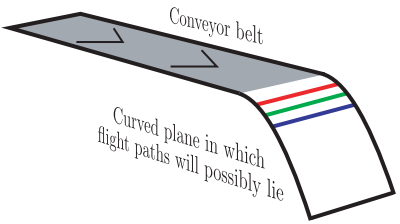

Fig. 3. Visualization of the three sensor lines of a trilinear line scan camera projected on the curved plane of possible flight paths. The gaps are shown larger than in reality for illustration purposes.

can use the number of time steps between observing the centroid in one channel and observing it in the other channels to determine the time that has passed between observing the centroid in the first, second, and (depending on the sensor layout) third and fourth channel. This temporal offset can then be combined with the spatial offset observed in the multiple channels to determine the particle's velocity.

This approach can be realized well in real-time. Compared with state-of-the-art optical belt sorters in which the particles are to be detected once, only twice as much image processing operations are required when using ColorTrack using two observations. Assigning the observations in the different color channels to one particle poses an additional overhead. However, the numbers of particles that are observed simultaneously by a line scan camera are commonly considerably lower than the numbers of particles observed by an area scan camera, making this step far cheaper than in the predictive tracking approach.

3 Implementation

To test our concept, we have created an implementation in Matlab that can read recordings of line scan camera images and generate predictions for each particle recorded. We wrote our implementation for trilinear line scan cameras to be able to evaluate the approach using an Advanced Camera Components (ACC) SAPPAN CL [14] line scan camera that we have at our disposal.

When recording images with a camera continuously, the time can be seen as an additional dimension [21, Ch. 1]. Usually, when applying image processing algorithms to image data obtained on belt sorters equipped with line scan cameras, a two-dimensional image is generated by concatenating the lines recorded at subsequent time steps. The resulting image of the particle obtained is similar to an image recorded by an area scan camera but it may appear stretched or shrunk along the temporal axis, depending on the sampling rate.

In our approach, we order the color channels on an additional dimension. This leads to a three-dimensional coordinate system as illustrated in Fig. 4. We denote the first axis along the pixels of the sensor as the x-axis and use t for the axis at which the line scan camera images are concatenated. The different color channels are ordered on the y-axis.

In all our illustrations given, the indexing of the pixels starts at the upper left of the image and the index increases along the x-axis horizontally and along the t-axis vertically. Furthermore, as illustrated in Fig. 4, we define a coordinate

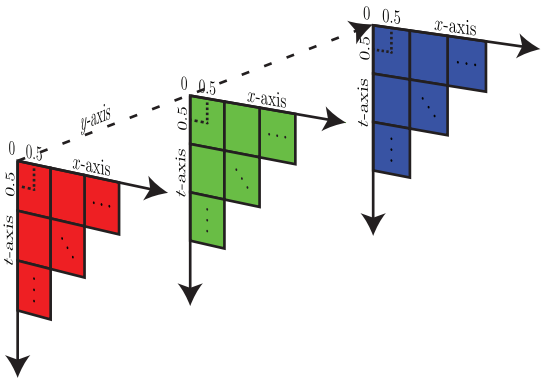

Fig. 4. Coordinate system comprising three axes.

system that allows subpixel indexing that starts on the upper left corner of the upper leftmost pixel.

Ordering the multiple color channels on the y-axis is motivated by the sensor layout of line scan cameras featuring a bi-, tri-, or quadlinear layout. As shown in Fig. 2a, Fig. 2b, and Fig. 2c, the sensor lines are lined up in parallel along the axis orthogonal to the x-axis. Thus, line scan cameras with these patterns feature a two-dimensional sensor array. As the sizes of the gaps are usually a multiple of the size of a pixel sensor, the line scan camera can be seen as an area scan camera of which we only observe certain pixels. Using a coordinate system that also takes the pixels left out in between into account, image coordinates can be projected into world coordinates in the same manner as for area scan cameras. As the sizes of the gaps between the color channels are camera specific, the coordinates along the y-axis depend heavily on the sensor layout of the line scan camera used.

The sensor layout of the ACC SAPPAN CL that we use in our evaluation is illustrated in Fig. 5. The sensor features a gap of seven pixel sizes between each pair of neighboring lines. To be compatible with bilinear layouts, we focus on using two color channels in our implementation: the red and the blue channel. These two channels are separated by a gap of the size of 15 pixels in the ACC SAPPAN CL.

3.1 Determining the Centroids Using Image Processing

In this subsection, we explain how to find the centroid of each particle in all color channels. For this, we regard two-dimensional images of the particles with

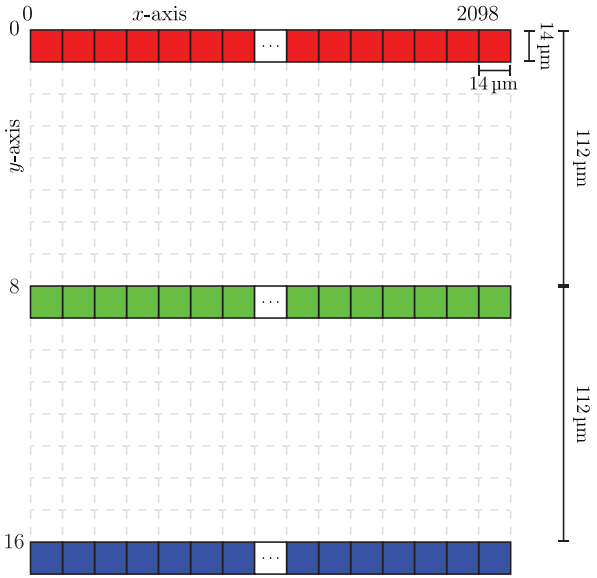

Fig. 5. Sensor layout of the ACC SAPPAN CL line scan camera according to the documentation [14].

the x-axis on one axis and (part of the) t-axis on the other. In our figures, we overlay all color channels without temporal correction for visualization purposes. In the implementation, all color channels are regarded separately.

An easy solution to calculate the centroid is to separate the object from the background using binarization and to then determine the particle's centroid based on the pixels occupied. An exemplary result of the binarization is shown in Fig. 6.

However, including the color intensities into the generation of the contour of the particle has proven to allow for a more accurate determination of the centroid. For this, we approximate the object as a series of edges as shown in Fig. 7. The edges were generated by interpolating the color intensities in the image and then tracing along the interpolated line of one specific color intensity. For all particles in one data set, the same intensity was used that was empirically chosen to result in little influence from imaging noise while ensuring that a large part of each particle is included in the shape.

To calculate the centroid of the particle approximated as a polygon, we first number the vertices clockwise from 1 to n. Then, we calculate the area occupied

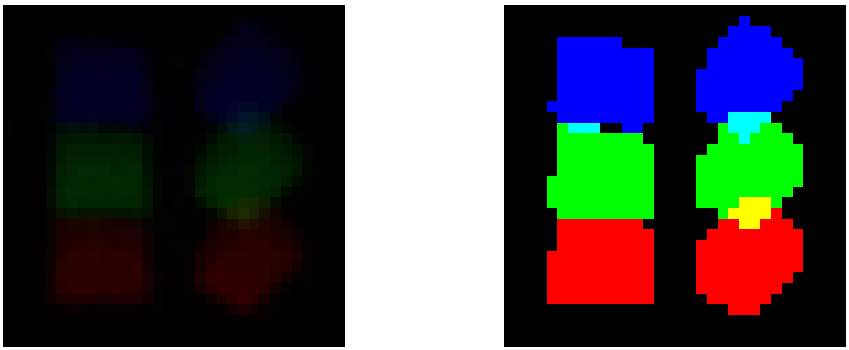

(a) Raw data.

(b) Result of the binarization.

Fig. 6. Visualization of the binarization. On the basis of the displacement on the horizontal axis, the particle on the left can be seen to not move straight in the transport direction.

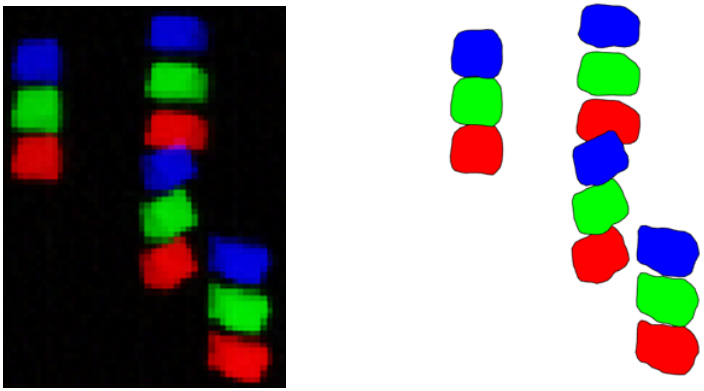

(a) Raw data modified for improved visibility.

(b) Shapes extracted from the raw data.

Fig. 7. Visualization of the approximation of the particles using polygons.

by the particle using the x and t-coordinates of each vertex x_i and t_i using [22]

$$a = \frac{1}{2}\sum_{i=1}^{n}(x_i t_{i+1} - x_{i+1} t_i) \ .$$

Afterward, we use the area to calculate the particle's centroid in image coordinates x^{im} and t^{im} via the formulae [22]

$$x^{\mathrm{im}} = \frac{1}{6a}\sum_{i=1}^{n}(x_i + x_{i+1})(x_i t_{i+1} - x_{i+1} t_i) \text{ and}$$
$$t^{\mathrm{im}} = \frac{1}{6a}\sum_{i=1}^{n}(t_i + t_{i+1})(x_i t_{i+1} - x_{i+1} t_i) \ .$$

Another possible approach to determine the centroid is to calculate an image moment over the region in which the particle is located and assume that the color intensities correspond to the mass of the object in this area [21, Ch. 7.2.2].

3.2 Calculating the Velocities

In order to calculate the velocities from the individual centroids, we have to find an assignment of each centroid observed in one color channel to one centroid in each other channel. Using a rough guess for the particle's movement, we were able to obtain reliable assignments. While the rough guess results in a non-negligible uncertainty as to where the centroid should be in the other channels, the extent of each particle was, in our experiments, always large enough to determine a point on the surface of the particle in the other color channels. We deem problems in the matching to only be of importance if the gaps in the sensor pattern are large and the particles are small and feature a lot of movement orthogonal to the transport direction.

Algorithmically, matching multiple observations to one particle can be implemented in the same way as in the predictive tracking approach, when using the rough velocity guess available to generate a prediction. We then have a problem in the form of linear assignment problem, for which fast solvers such as LAPJV [23] and the auction algorithm [24] are available. While the problem scales cubically in the number of particles, the field of view of a line scan camera can only contain numbers of particles that result in problem sizes that can still be solved easily in real-time by current desktop PCs.

Having determined the centroids of a particle in all color channels in image coordinates, we can now use the coordinates of the centroids to get an estimate of the particle's velocity. For this, we need the sampling frequency, intrinsic

parameters of the camera and the lens, and some information about the extrinsic calibration. First, we need to determine the time that has passed between observing the particle in one channel and observing it in the next. Since we have disabled the temporal offset for the different lines of the line scan camera, the time that has passed between the observations is directly proportional to the distance along the t-axis. As there is no optical distortion in the t-coordinate, we can first determine the distance along the t-axis between the centroids in the individual color channels in the image coordinate system. Afterward, we only have to multiply the distance by the reciprocal of the sampling frequency, e.g., by 0.5 ms when the sampling rate is 2 kHz.

For all compatible sensor layouts, only two color channels need to be used. In our implementation, we use the red and the blue color channel as this results in the largest gap between the lines of the sensor. We use t^{im} to denote the time coordinate at which the centroid was detected in one color channel in image coordinates and t^{w} to denote the corresponding time in world coordinates, meaning the actual time that has passed since the first line was recorded. In the following, we use the lower indices b, g, and r to indicate in which color channel the detection occurred. We can calculate the temporal offset $\Delta t^{\mathrm{w}}_{\mathrm{r,b}}$ between spotting the particle in the red and the blue color channel in world coordinates via

$$\Delta t^{\mathrm{w}}_{\mathrm{r,b}} = \frac{t^{\mathrm{im}}_{\mathrm{b}} - t^{\mathrm{im}}_{\mathrm{r}}}{\text{sampling frequency}} \ .$$

Having the temporal offset at our disposal, we now further require some parameters of the extrinsic calibration. One way to approximate the required information is to use a camera calibration pattern for line scan cameras [25] and place the calibration pattern where the particles are expected to pass by. However, the parameters can only be approximated as the distance between the particles and the camera may differ as the height of the particles when they pass the sensor during the flight phase may vary. There are also other ways to approximate the parameters of the calibration, such as deriving parameters from recordings of particles with known extent or approximating the parameters manually by measuring. Furthermore, approaches to approximate the required parameters that are more experimentally-driven could also be employed.

Irrespective of how the calibration was approximated, a projection of image to world coordinates has to be derived. The different lines may correspond to up to four lines along the flight parabola. An illustration of the three lines present when using a scan camera with a trilinear pattern is given in Fig. 3. As the lines do not lie in a single plane in general, multiple extrinsic calibrations may be necessary. We use $\pi(\cdot)$ for the projection that uses the correct calibration to map

image to world coordinates according to

$$\begin{bmatrix} x^{\mathrm{w}} \\ y^{\mathrm{w}} \end{bmatrix} = \pi \left(\begin{bmatrix} x^{\mathrm{im}} \\ y^{\mathrm{im}} \end{bmatrix} \right) .$$

To approximate the velocity of a particle, we need to use the centroids in two color channels. As previously mentioned, we use the red and the blue color channel of our trilinear line scan camera as the two lines observed are the furthest apart. We can approximate the velocities $\dot{x}^{\mathrm{w}}$ and $\dot{y}^{\mathrm{w}}$ in world coordinates using the coordinates of the centroids in the blue and the red color channel (indexed by b and r) via the formula

$$\begin{bmatrix} \dot{x}^{\mathrm{w}} \\ \dot{y}^{\mathrm{w}} \end{bmatrix} = \frac{1}{\Delta t^{\mathrm{w}}_{\mathrm{r,b}}} \left(\pi \left(\begin{bmatrix} x^{\mathrm{im}}_{\mathrm{b}} \\ y^{\mathrm{im}}_{\mathrm{b}} \end{bmatrix} \right) - \pi \left(\begin{bmatrix} x^{\mathrm{im}}_{\mathrm{r}} \\ y^{\mathrm{im}}_{\mathrm{r}} \end{bmatrix} \right) \right) .$$

4 Evaluation

For our evaluation, we recorded multiple data sets using an area scan camera and a line scan camera simultaneously. We recorded data sets both on a large industrial-scale optical belt sorter and on our small-scale optical belt sorter used for rapid prototyping called TableSort. The belt of the former ran at a velocity of approximately 2.7 m/s and the belt of the latter ran at approximately 1.1 m/s. No ground truth data of the movement of the particles was recorded as this was deemed infeasible. Instead, we used our predictive tracking approach [6] on the image data captured using the area scan camera (Allied Vision Technologies Bonito CL-400) to provide a reference to compare with.

The setup of the sorters used for recording the image data is illustrated in Fig. 8. For both sorters, the fields of view of the line scan camera and area scan camera did not overlap and we did not have a perfect calibration between the two cameras. While we deem it possible to combine calibration patterns of line scan cameras [25] and area scan cameras into one calibration pattern to attain a calibration of the line scan camera to the area scan camera, we have not used any sophisticated approaches and instead performed an approximate manual calibration, which was then improved using the data recorded.

The particles passed the field of view of the area scan camera before being observed by the line scan camera. To match the particles in the recordings of the two cameras, we generated a prediction as to when and where each particle will pass the line scan camera based on the data observed by the area scan camera. We then determined the matching that minimizes the sum of the distances between

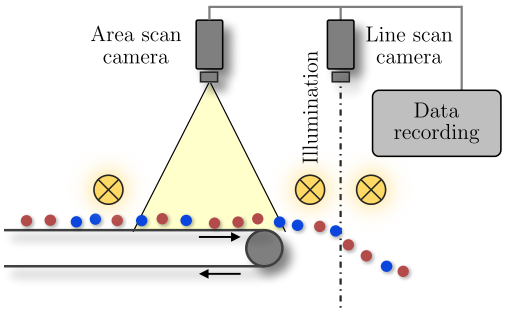

Fig. 8. Layout of the sorters used for recording the data for the evaluation.

these predictions and the actual positions at which the particles were observed by the line scan camera.

We evaluated the approaches based on two criteria that are laid out in the next subsection. As bulk materials to evaluate, we used cuboid-shaped plastic granule as shown in Fig. 9a on the industrial-scale sorter in the first scenario and spherically-shaped airsoft ammunition (commonly referred to as BB) as shown in Fig. 9b on both the industrial-scale sorter and TableSort in the second and third scenario. The third scenario also features an additional disturbance in the form of a current of air disrupting the motion of the particles. The results were calculated based on the performance achieved for 682 particles in the first scenario, 310 in the second scenario, and 121 in the third. These numbers only include particles that were successfully matched between the recordings of the line scan camera and of the area scan camera.

While the particles of the granule are expected to settle on the belt and adapt to the belt velocity accurately, the particles of the BB feature more motion relative to the belt. The granule as a highly cooperative bulk material is well suited to the use of the prediction straight in the transport direction. Therefore, we do not expect a significant benefit to using the ColorTrack approach for this bulk material. The BB behave less cooperatively and thus a significant improvement is expected for this bulk material. We did not mix bulk materials and only evaluated the precision of the predictions to be able to give an assessment of the reliability of the separation process.

4.1 Evaluation Criteria

As we do not have an accurate calibration between the line scan camera and the area scan camera, we are unable to map specific coordinates in one camera

(a) Granules used as bulk material.

(b) Spherically-shaped BB used as bulk material.

Fig. 9. Photographs of the bulk materials used.

coordinate system to the coordinate system of the other camera. Therefore, we use an aspect of the prediction that can be compared reliably even without an accurate calibration. To assess the quality of the prediction, we determine the accuracy of the angle on the $x^{\mathrm{w}}y^{\mathrm{w}}$-plane. This criterion is invariant under translation and scaling without requiring strong assumptions. The deviation is given as the difference between the estimated angle and the reference angle. Close care needs to be taken when calculating measures of the deviation on angular quantities [26, Ch. 1.3.2], but the small angles in our application do not necessitate adjustments.

The edges of the field of view of the area scan camera were aligned parallel and orthogonal to the transport direction. As in actual bulk sorting tasks, the line scan camera observed a line (or, to be precise, multiple lines) orthogonal to the transport direction. The precision of the alignment, however, was limited due to the manual installation of the cameras. As no precise calibration was available, we used our data combined with assumptions to compensate the difference in the orientation between the line scan camera and area scan camera. For this, we first assumed that the mean of the angular errors is zero and shifted the angles so that the mean of the predicted angles and the reference angles became equal. For low numbers of particles, this assumption would significantly skew our assessment. Since more than 100 particles were regarded in each scenario, the assumption does not have a major impact on the evaluation results.

A more important aspect affecting this evaluation of the angle is the imprecise reference that the error is based on. The error $\mathrm{Err}_{\mathrm{Eval}}$ determined in our evaluation is partly composed of the error $\mathrm{Err}_{\mathrm{PT}}$ of the prediction provided by the predictive tracking that we use as a reference and partly of the error $\mathrm{Err}_{\mathrm{CT}}$ of the ColorTrack approach. Due to this additional component, the actual error of the ColorTrack approach is expected to be lower than the error calculated based on this reference

as

$$\mathrm{Err}_{\mathrm{Eval}} \geq \mathrm{Err}_{\mathrm{PT}} + \mathrm{Err}_{\mathrm{CT}}$$

holds on average, unless there is a reason to believe that the errors cancel out.

To get an impression of how much of the deviation is caused by the predictive tracking and to give a reference, we approximate $\mathrm{Err}_{\mathrm{PT}}$ in a similar way as in [6]. For this, we artificially introduce a prediction phase in the tracking based on the area scan camera images during which measurements of the particle's position are intentionally disregarded and only predictions are performed. By comparing the prediction based on part of the measurements with the result of the tracking based on all measurements, we can assess the quality of the prediction. Due to the limited usable area in the images of the area scan camera, the prediction horizon was chosen to be 6 cm.

To evaluate the old model of performing a prediction straight in the transport direction, the angle for each prediction is chosen to be the mean of the reference angles for all particles. This choice minimizes the mean squared error and is thus favorable to the old model that we aim to outperform using the ColorTrack approach.

Based on the angles and positions determined, we provide a second criterion to give an impression of the impact that the deviations in the angles have on the separation. For this criterion, we integrate the actual aim to perform an accurate separation using the array of compressed air nozzles into the evaluation. Using knowledge of the setup of the optical belt sorters, we try to assess what percentage of the particles would be hit under certain assumptions, given the reference and the estimated angle.

This criterion heavily depends on the size of the nozzles and on the distance between the start of the prediction and the array of nozzles. For both sorters, we used the distances and the numbers of nozzles that are present when the sorters are used for actual sorting. In the industrial-scale sorter, the array of nozzles measured 70 cm, comprising 128 nozzles at a distance of 12 cm to the start of the prediction phase. In TableSort, the array measured 16 cm and featured 16 nozzles located at a distance of 15 cm from the start of the prediction phase.

To calculate the percentage of particles hit, we make a couple of assumptions and perform approximations as illustrated in Fig. 10. We say that the array of compressed air nozzles is subdivided into multiple equally sized parts that are precisely covered by that nozzle. For simplicity, we assume that the array of nozzles is only a line and has no extent along the transport direction. The flight paths of the particle based on the reference angle and the estimated angle are determined and the intersections with the array of compressed air nozzles are calculated. The nozzle that would be activated and the nozzle that

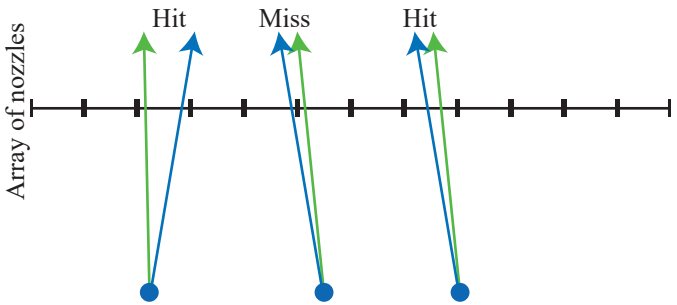

Fig. 10. Illustration how the hit ratio is calculated in the evaluation. The blue arrow shows the expected flight path of the particle and the green arrow shows the true flight path. Only a few nozzles are shown and the lengths are not drawn to scale.

should be activated are then determined based on the intersections. If the correct nozzle would be activated for the respective particle, the separation is considered successful, otherwise, it is deemed unsuccessful. Only one nozzle is activated for each particle. This leads to lower hit ratios than can be observed in practice as it is common practice to activate multiple nozzles. Especially if the particle of the bulk material is expected to pass by in the middle of two nozzles or at the edge of one nozzle, activating the neighboring nozzle significantly increases the probability of hitting the object. For simplicity, we employ the straightforward strategy to only activate a single nozzle, which is a strategy that can be used to save air pressure (and thus costs) and reduce by-catch.

4.2 Evaluation Results

The evaluation results for the error in the angle are shown as boxplots in Fig. 11. Boxplots are a very expressive way to visualize the deviations as the ranges in which the error commonly lies is evident. The red lines in the middle of the boxes show the median while the boxes show the range from the 25th percentile to the 75th percentile and thus contain 50% of all values. All values that deviate more than $\pm 2.7\sigma$ from the median (covering approximately 99.3% of all deviations when the data is normally distributed) are considered outliers. The whiskers (the lines that go beyond the boxes) extend to the furthest point that is not considered to be an outlier. The whiskers can be conveniently used to determine how many additional nozzles should be activated to achieve a hit ratio of about 99%. Outliers were omitted in the boxplots as plotting them would induce the

need for different axes ranges and reduce the clarity of the presentation in the plots.

In Fig. 11a, the results of the predictive tracking for a 6 cm prediction phase are shown. It can be seen that the predictions for almost all particles are correct up to an angle of ±0.4° for the two scenarios featuring the industrial-scale sorter. For the scenario using the TableSort system, the error is within the range of −0.3° and 1.4° for almost all particles. There is a significant bias in this scenario caused by the external disturbance in form of a current of air that disturbs the motion of the particles and accelerates them in one direction.

In Fig. 11b, we show the angular errors for the prediction straight in the transport direction when the result of predictive tracking is used as the reference. The error is between −0.8° and 0.8° for almost all particles in the first scenario, which is the scenario best suited for the old prediction model due to the cooperative behavior of the granules. In the second scenario featuring the BB, the deviation is almost always between −1.5° and 1.5° and is thus considerably higher. In the third scenario, in which the TableSort system is used, the error is between −3.5° and 3.6° for almost all particles. The median is always close to zero as our calibration ensured that the mean of the errors is zero.

Fig. 11c shows the deviations between the angles obtained using predictive tracking and those obtained using the ColorTrack approach. The error in the angle in the first scenario is between −0.8° and 0.9° for almost all particles. In this scenario, the prediction straight in the transport direction slightly outperforms the ColorTrack approach. This shows the limitations of the ColorTrack approach—the precision of the approach is limited by the quality of the image acquisition and the suitability of the assumptions. If the bulk material is very cooperative, resulting in a very low variation of the angles, assuming the angle to be zero can lead to a lower deviation than that caused by the imprecision of the ColorTrack approach. Thus, using the ColorTrack approach may only pay off if the variation in the angles is sufficiently high.

In the second scenario that is significantly harder, the ColorTrack approach can be seen to provide good results. With an error between −0.9° and 1.0° for almost all particles, using ColorTrack results in a performance close to the performance achieved for the very cooperative granules. Compared with the prediction straight in the transport direction, the superiority of the ColorTrack approach is evident. The deviation in the third scenario, in which the TableSort system was used, is almost always between −2.1° bis 1.8°. This is also a significant improvement when compared with the performance achieved using the prediction straight in the transport direction.

The hit ratios determined in the second part of the evaluation are in accordance with the angular errors observed. As shown in Tab. 1, the hit ratio is

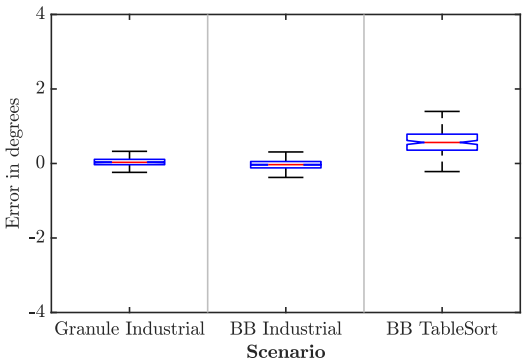

(a) Error in the angles when using the predictive tracking approach that requires an area scan camera.

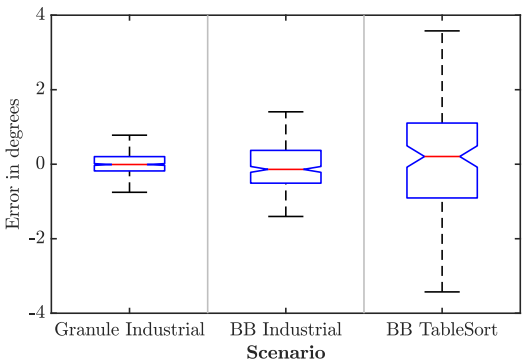

(b) Error in the angles when the prediction straight in the transport direction is used.

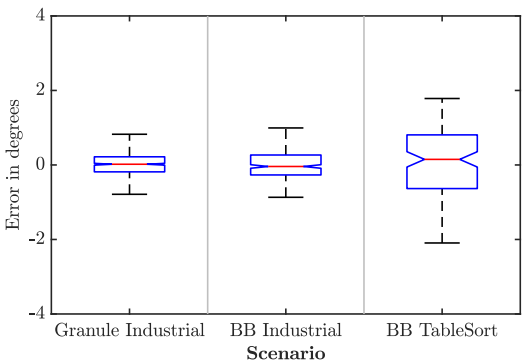

(c) Error in the angles when using the ColorTrack approach.

Fig. 11. Errors in the angles for the three approaches applied to the three scenarios shown as boxplots.

	Granules Industrial	BB Industrial	BB TableSort
Prediction in the transport direction	91.50%	79.35%	73.55%
Prediction of ColorTrack	88.42%	87.42%	82.64%

Table 1. Hit ratios for the prediction straight in the transport direction and the ColorTrack approach for the three scenarios.

slightly better for the prediction straight in the transport direction in the first scenario. For the second and the third scenario featuring BB, the hit ratio is significantly higher when using the ColorTrack approach.

All in all, our evaluation shows that the ColorTrack approach improves the separation process if the bulk material is not highly cooperative. We expect the advantage of the ColorTrack approach to be even more pronounced for bulk materials that feature even more motion orthogonal to the transport direction, such as peppercorns.

5 Conclusion

In this paper, we have shown that the chromatic offset of line scan cameras can be used effectively in the context of optical belt sorters to improve the predictions of the particles' flight paths when the bulk material features significant motion orthogonal to the transport direction. The improved prediction quality of our novel approach allows improving the separation process while requiring neither much more computational power for real-time implementations nor additional hardware, which are required by the approach presented in [6]. Thus, our approach can be used to improve existing systems without a need for hardware modifications. Furthermore, the ColorTrack approach can be employed when the high frame rate and resolution of line scan cameras is required that cannot be matched by today's area scan cameras.

The proposed approach is a modification that can be applied to state-of-the-art optical belt sorters to improve cost efficiency, e.g., by reducing the amount of compressed air required, while only necessitating algorithmic improvements and a sufficiently fast computer. As future work, we aim to consider other improvements that can be made using only algorithmic innovations, such as optimizing which additional nozzles are to be activated to achieve a desired hit ratio. Rather than regarding all particles of the bulk material individually, taking a whole series of particles into account can help to improve the hit ratio while minimizing

by-catch. Furthermore, more effort will go into data-driven calibration, which could result in, e.g., an optical belt sorter using predictive tracking that can automatically calibrate itself.

Acknowledgment: The IGF project 18798 N of the research association Forschungs-Gesellschaft Verfahrens-Technik e.V. (GVT) was supported via the AiF in a program to promote the Industrial Community Research and Development (IGF) by the Federal Ministry for Economic Affairs and Energy on the basis of a resolution of the German Bundestag.

The authors would like to thank the students Christian Tesch and Ulrich Berger, who significantly contributed to the realization of this project.

References

[1] Hermann Wotruba. Stand der Technik der sensorgestützten Sortierung (in German). *BHM Berg- und Hüttenmännische Monatshefte*, 153:221–224, June 2008.

[2] Joseph Irudayaraj and Christoph Reh. *Nondestructive Testing of Food Quality*, volume 18. John Wiley & Sons, 2008.

[3] Mark Graves and Bruce Batchelor. *Machine Vision for the Inspection of Natural Products*. Springer Science & Business Media, 2003.

[4] Felix Brandt and Reiner Haus. New Concepts for Lithium Minerals Processing. *Minerals Engineering*, 23(8):659–661, 2010.

[5] Raffaella Mattone, Giuseppina Campagiorni, and Filippo Galati. Sorting of Items on a Moving Conveyor Belt. Part 1: A Technique for Detecting and Classifying Objects. *Robotics and Computer-Integrated Manufacturing*, 16(2):73–80, 2000.

[6] Florian Pfaff, Marcus Baum, Benjamin Noack, Uwe D. Hanebeck, Robin Gruna, Thomas Längle, and Jürgen Beyerer. TrackSort: Predictive Tracking for Sorting Uncooperative Bulk Materials. In *Proceedings of the 2015 IEEE International Conference on Multisensor Fusion and Integration for Intelligent Systems (MFI 2015)*, San Diego, California, USA, September 2015.

[7] Florian Pfaff, Christoph Pieper, Georg Maier, Benjamin Noack, Harald Kruggel-Emden, Robin Gruna, Uwe D. Hanebeck, Siegmar Wirtz, Viktor Scherer, Thomas Längle, and Jürgen Beyerer. Improving Optical Sorting of Bulk Materials Using Sophisticated Motion Models. *tm - Technisches Messen, De Gruyter*, 83(2):77–84, February 2016.

[8] Christoph Pieper, Georg Maier, Florian Pfaff, Harald Kruggel-Emden, Siegmar Wirtz, Robin Gruna, Benjamin Noack, Viktor Scherer, Thomas Längle, Jürgen Beyerer, and Uwe D. Hanebeck. Numerical Modeling of an Automated Optical Belt Sorter Using the Discrete Element Method. *Powder Technology*, July 2016.

[9] Florian Pfaff, Christoph Pieper, Georg Maier, Benjamin Noack, Harald Kruggel-Emden, Robin Gruna, Uwe D. Hanebeck, Siegmar Wirtz, Viktor Scherer, Thomas Längle, and Jürgen Beyerer. Simulation-Based Evaluation of Predictive Tracking for Sorting Bulk Materials. In *Proceedings of the 2016 IEEE International Conference on Multisensor*

Fusion and Integration for Intelligent Systems (MFI 2016), Baden-Baden, Germany, September 2016.

[10] Georg Maier, Florian Pfaff, Christoph Pieper, Robin Gruna, Benjamin Noack, Harald Kruggel-Emden, Thomas Längle, Uwe D. Hanebeck, Siegmar Wirtz, Viktor Scherer, and Jürgen Beyerer. Fast Multitarget Tracking via Strategy Switching for Sensor-Based Sorting. In *Proceedings of the 2016 IEEE International Conference on Multisensor Fusion and Integration for Intelligent Systems (MFI 2016)*, Baden-Baden, Germany, September 2016.

[11] Bahadir K. Gunturk, John Glotzbach, Yucel Altunbasak, Ronald W. Schafer, and Russel M. Mersereau. Demosaicking: Color Filter Array Interpolation. *IEEE Signal Processing Magazine*, 22:44–54, January 2005.

[12] Understanding Line Scan Camera Applications. Technical report, Teledyne Dalsa, 2014.

[13] Andreas Lange. Bi, Tri, and Multi-Line Imaging for Color Inspection. Presentation, May 2014.

[14] ACC Advanced Camera Components GmbH. *User Manual for the CCD Color Line Scan Camera SAPPAN CL (in German)*, August 2005. Rev. 1.4.

[15] Teledyne DALSA. *User Manual for Piranha4 Color 2k and 4k Cameras*, June 2015. Rev. 03.

[16] e2v. *User Manual for ELiiXA UC4/UC8 Cameras*, June 2016. Rev. H.

[17] Teledyne DALSA. *User Manual for Piranha4 RGB + NIR / Monochrome Cameras*, September 2015. Rev. 00.

[18] Teledyne DALSA. *User Manual for Spyder3 SG-34 Color 2k and 4k Cameras*, July 2014. Rev. 02.

[19] e2v. *User Manual for UNiiQA+ Color Cameras*, September 2016. Rev. I.

[20] e2v. *User Manual for AViiVA SC2 LV Color LineLine Cameras*, June 2016. Rev. H.

[21] Alan C. Bovik. *Handbook of Image and Video Processing*. Academic Press, 2010.

[22] Paul Bourke. Calculating the Area and Centroid of a Polygon. *Swinburne University of Technology*, 1988.

[23] Roy Jonker and Anton Volgenant. A Shortest Augmenting Path Algorithm for Dense and Sparse Linear Assignment Problems. *Computing*, 38(4):325–340, 1987.

[24] Dimitri P. Bertsekas. *Encyclopedia of Optimization*, chapter Auction Algorithms, pages 128–132. Springer, 2 edition, 2009.

[25] Carlos A. Luna, Manuel Mazo, José Luis Lázaro, and Juan F. Vazquez. Calibration of Line-Scan Cameras. *IEEE Transactions on Instrumentation and Measurement*, 59(8):2185–2190, 2010.

[26] S. Rao Jammalamadaka and Ambar Sengupta. *Topics in Circular Statistics*. World Scientific, 2001.